

# Dynamical Mechanisms of Odor Processing in Olfactory Bulb Mitral Cells

Daniel B. Rubin and Thomas A. Cleland

Department of Neurobiology and Behavior, Cornell University, Ithaca, New York

Submitted 10 March 2006; accepted in final form 21 March 2006

**Rubin, Daniel B. and Thomas A. Cleland.** Dynamical mechanisms of odor processing in olfactory bulb mitral cells. *J Neurophysiol* 96: 555–568, 2006. First published May 17, 2006; doi:10.1152/jn.00264.2006. In the olfactory system, the contribution of dynamical properties such as neuronal oscillations and spike synchronization to the representation of odor stimuli is a matter of substantial debate. While relatively simple computational models have sufficed to guide current research in large-scale network dynamics, less attention has been paid to modeling the membrane dynamics in bulbar neurons that may be equally essential to sensory processing. We here present a reduced, conductance-based compartmental model of olfactory bulb mitral cells that exhibits the complex dynamical properties observed in these neurons. Specifically, model neurons exhibit intrinsic subthreshold oscillations with voltage-dependent frequencies that shape the timing of stimulus-evoked action potentials. These oscillations rely on a persistent sodium conductance, an inactivating potassium conductance, and a calcium-dependent potassium conductance and are reset via inhibitory input such as that delivered by periglomerular cell shunt inhibition. Mitral cells fire bursts, or clusters, of spikes when continuously stimulated. Burst properties depend critically on multiple currents, but a progressive deinactivation of  $I_A$  over the course of a burst is an important regulator of burst termination. Each of these complex properties exhibits appropriate dynamics and pharmacology as determined by electrophysiological studies. Additionally, we propose that a second, inconsistently observed form of infrathreshold bistability in mitral cells may derive from the activation of ATP-activated potassium currents responding to hypoxic conditions. We discuss the integration of these cellular properties in the larger context of olfactory bulb network operations.

## INTRODUCTION

Mitral cells, along with middle and deep tufted cells, are the principal output neurons of the olfactory bulb. They receive direct afferent synaptic input from hundreds to thousands of primary olfactory sensory neurons (OSNs) and integrate these inputs both with indirect afferent inputs transformed via a heterogeneous population of juxtglomerular interneurons (Cleland and Sethupathy 2006) and with the activity of centrifugal cortical and modulatory projections (Fig. 1A). As mitral cell ensemble activity largely constitutes the output of the olfactory bulb, it has been termed the “secondary olfactory representation” (Cleland and Linster 2005; Cleland and Sethupathy 2006); furthermore, as this representation is delivered to  $\geq 10$  cortical and subcortical destinations via divergent axon collaterals (Cleland and Linster 2003), it is the last representation in the olfactory pathway to necessarily contain a full complement of afferent sensory information. Consequently, the mitral cell has received a great deal of research attention, and a number of its interesting anatomical and physiological spe-

cializations have been studied. However, owing in part to ongoing debate about the role of the olfactory bulb in odor processing, as well as the complexities of integrating data across levels of analysis, studies have tended to focus exclusively either on cellular properties or on network phenomena. As it becomes increasingly clear that olfactory representations include both channel-coding (“which neurons are active?”) and dynamical (“what is the timing of their activity?”) elements, it is correspondingly essential to understand the contributions of specialized cellular properties to the representational and processing capabilities of the bulbar network.

Mitral cells can exhibit intrinsic bistable and oscillogenic properties that influence their responses to specific odor stimuli (Balu et al. 2004; Chen and Shepherd 1997; Desmaisons et al. 1999; Heinbockel et al. 2004; Heyward et al. 2001). For example, olfactory bulb slice experiments have revealed that subthreshold oscillations in mitral cells can influence the timing of spontaneous and evoked action potentials (Desmaisons et al. 1999). Network interactions among activated bulbar neurons are also believed to contribute to spike timing and synchronization among mitral cells (Friedman and Strowbridge 2003; Hayar et al. 2005; Kashiwadani et al. 1999; Lagier et al. 2004; Nusser et al. 2001). Although all of these channel-coding and dynamical phenomena are likely to contribute to odorant representations, it is not yet clear how they can be interrelated or what part each may play under differing circumstances. To better interrelate complex cellular and network-level datasets, and hence strengthen experimental hypotheses, we sought to develop a computational model of the olfactory bulb mitral cell that could exhibit complex cellular properties such as subthreshold oscillations and appropriate pharmacological responses using biophysical mechanisms, while still remaining computationally tractable for incorporation into network models. We first illustrate the model cell’s ability to replicate diverse complex responses measured in mitral cells and subsequently use the model to deconstruct the biophysical bases of certain of these properties, proposing testable hypotheses of mechanism. In particular, we illustrate putative mechanisms underlying the slow bursting properties of mitral cells and propose an explanation for the dissimilar patterns of membrane bistability reported by different laboratories.

## METHODS

### Model principles

The mitral cell model described herein was shaped by four principal objectives. First, the model must represent cellular morphological and

Address for reprint requests and other correspondence: T. A. Cleland, Dept. Neurobiology and Behavior, Cornell University, Ithaca, NY 14853 (E-mail: tac29@cornell.edu).

The costs of publication of this article were defrayed in part by the payment of page charges. The article must therefore be hereby marked “advertisement” in accordance with 18 U.S.C. Section 1734 solely to indicate this fact.

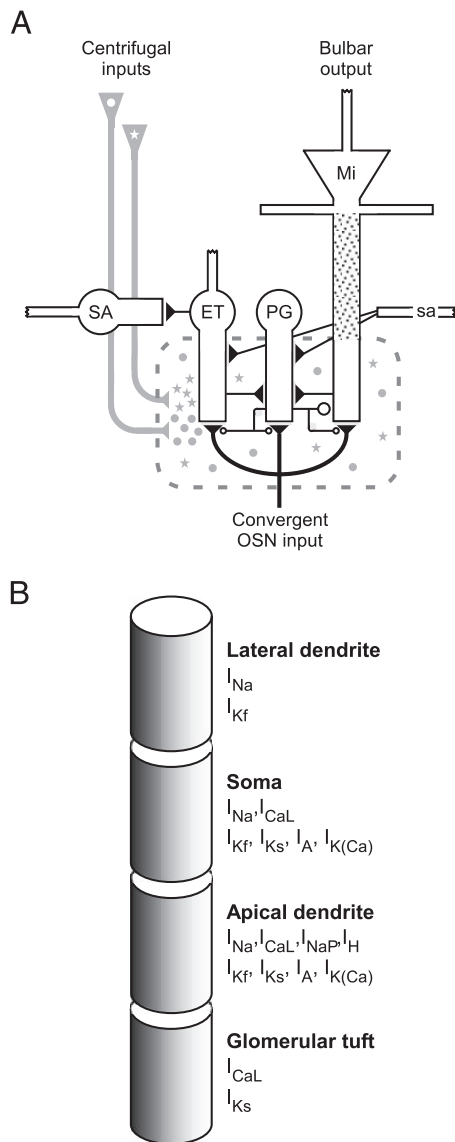


FIG. 1. Model architecture. *A*: schematic of olfactory bulb glomerular network, illustrating direct activation of mitral cells by olfactory sensory neurons [convergent olfactory sensory neuron (OSN) input] as well as shunt inhibition of mitral cell dendrites by periglomerular (PG) neuron spines activated by the same sensory input. Presynaptic inhibition of OSN terminals by PG cells is also depicted. Mi., mitral cell; ET, external tufted cell; SA, short-axon cell; sa, axon of short-axon cell. Central modulatory inputs are also depicted. Stippling denotes mitral cell apical dendrite; dotted line denotes the boundary of the glomerulus. Adapted from Cleland and Sethupathy (2006). *B*: schematic of 4-compartment mitral cell model and its membrane mechanisms (inward and outward currents).  $I_{Na}$ , sodium spike current;  $I_{CaL}$ , L-type high-voltage-activated calcium current;  $I_{NaP}$ , persistent sodium current;  $I_H$ , hyperpolarization-activated cation current;  $I_{Kf}$ , fast delayed rectifier potassium current;  $I_{Ks}$ , slow delayed rectifier potassium current;  $I_A$ , inactivating potassium current, including slower variant known as D-current;  $I_{K(Ca)}$ , calcium-dependent potassium current.

physiological properties with adequate accuracy and precision for its intended purposes. Second, it must be computationally efficient, such that moderately sized networks can be constructed and employed toward useful ends. Third, it should be reasonably compartmentalized, so that elements of the model can be upgraded or redesigned as required without rendering the revised model incompatible with its predecessors. Fourth, although the point of compartmental models is

to depict cellular properties in biophysical detail, we hold an explicit bias against the addition of unconstrained variables; excess free parameters can improve apparent fits to data but will reduce models' predictive value.

### Model morphology and passive properties

We based the present model (Fig. 1*B*) on the four-compartment mitral cell model of Davison and colleagues (2000), adding additional current mechanisms and adjusting parameters so as to replicate the complex dynamical properties of mitral cells observed in studies of rat olfactory bulb slices (Balu et al. 2004; Chen and Shepherd 1997; Desmaisons et al. 1999; Heyward et al. 2001). The Davison model abstracts the mitral cell into four isopotential compartments (glomerular tuft, apical dendrite, soma, and lateral dendrite), each possessing independent membrane properties and current complements and connected to one another by axial resistors. The complement and distribution of its membrane current mechanisms were derived from the 286-compartment model of Bhalla and Bower (1993), which in turn was closely based on mitral cell morphology and fit to current-clamp electrophysiological recordings under a broad variety of conditions. In Davison's reduced model, the lengths of the four compartments are identical, whereas their diameters differ so as to yield sections with empirically appropriate surface areas (glomerular tuft: 8,399.99  $\mu\text{m}^2$ ; apical dendrite: 32,801.4  $\mu\text{m}^2$ ; soma: 5,100.1  $\mu\text{m}^2$ ; lateral dendrite: 53,699.2  $\mu\text{m}^2$ ). The linking conductances between the four compartments are also unchanged from Davison: tuft to apical dendrite: 58.6  $\mu\text{S}$ ; apical dendrite to soma: 54.7  $\mu\text{S}$ ; soma to lateral dendrite: 194.0  $\mu\text{S}$ . Owing to extensive parameter optimization with respect to the model of Bhalla and Bower (1993), the reduced model faithfully replicates many aspects of mitral cell physiology (Davison et al. 2000).

The present model (Fig. 1*B*) inherits this reduced morphology and six channel mechanisms from its predecessors (Bhalla and Bower 1993; Davison et al. 2000): a fast sodium spike current ( $I_{Na}$ ), an L-type calcium current ( $I_{CaL}$ ), two delayed rectifier potassium currents distinguished by their activation kinetics ( $I_{Kf}$ ,  $I_{Ks}$ ), an inactivating potassium current (nominally  $I_A$ , but with slow inactivation kinetics rendering it intermediate between classical A- and D-current kinetics), and a calcium-activated potassium current ( $I_{K(Ca)}$ ). The model additionally incorporates a persistent sodium current mechanism ( $I_{NaP}$ ) adapted from that of Fransén and colleagues (2004), pursuant to the essential role of this current in mitral cell subthreshold oscillations (Balu et al. 2004; Desmaisons et al. 1999) as well as a hyperpolarization-activated cation current ( $I_H$ ) adapted from that of Saraga and colleagues (2003), and an ohmic ATP-sensitive potassium current ( $I_{K(ATP)}$ ). We adjusted the potassium and sodium reversal potentials to reported values, but otherwise retained the passive properties of the Davison model (Table 1). The conductance densities and distributions of membrane mechanisms were reparameterized as described below and are summarized in Table 2.

The current through each channel is determined at every time step through the Hodgkin-Huxley formalism (Hodgkin and Huxley 1952)

TABLE 1. Passive membrane parameters

Parameter	Value
$C_m$	1.0 $\mu\text{F}/\text{cm}^2$
$R_m$	10 $\text{k}\Omega/\text{cm}^2$
$E_{\text{leak}}$	-65 mV
$E_{Na}$	+55 mV
$E_K$	-90 mV
$E_{Ca}$	+70 mV
$E_H$	0 mV

TABLE 2. Active channel conductance densities ( $S/cm^2$ )

Compartment	$G_{Na}$	$G_{CaI}$	$G_{Kf}$	$G_{Ks}$	$G_A$	$G_{K(Ca)}$	$G_{NaP}$	$G_H$	$G_{K(ATP)}$
Soma	1.3532	0.004	0.1956	0.0028	0.012	0.12	—	—	—
Apical dendrite	0.00534	0.004	0.00123	0.00174	0.00735	0.1	0.00042	0.0024	0.0001
Lateral dendrite	0.0226	—	0.033	—	—	—	—	—	—
Glomerular tuft	—	0.0095	—	0.02	—	—	—	—	—

$$I_x = (G_{max})(m^a)(h^b)(V_m - E_x)$$

$$dm/dt = (m_\infty - m)/\tau_m$$

$$dh/dt = (h_\infty - h)/\tau_h$$

where for each channel type  $x$ ,  $G_{max}$  is the maximum conductance density of that channel in the designated compartment (Table 2),  $m$  and  $h$  are the activation and inactivation gating coefficients (of order  $a$  and  $b$ , respectively),  $V_m$  is the membrane potential within that compartment, and  $E_x$  is the reversal potential of the permeant ion(s). Each gating coefficient is calculated from a differential function of its steady state ( $\infty$ ) and time constant ( $\tau$ ), both of which are functions of voltage. The exception is the gating parameter for the  $I_{K(Ca)}$  current, which is a function of both voltage and the internal perimembrane calcium concentration. Perimembrane calcium concentration is modeled as decaying exponentially to a base level after calcium influx, using a mechanism modified from that of Destexhe and colleagues (1998).

### Computational methods and parameterization

All simulations were run in NEURON version 5.6 (<http://www.neuron.yale.edu>) (Carnevale and Hines 2006; Hines and Carnevale 1997, 2001) with a 0.01-ms time step. The change in voltage in each compartment was calculated as the sum of all ionic currents, injected currents, and currents flowing from the neighboring compartments. For example, in the apical dendrite:

$$C_m(dV_a/dt) = -I_{leak} - I_{Na} - I_{CaI} - I_{Kf} - I_{Ks} - I_A - I_{K(Ca)} - I_{NaP} - I_H - I_{K(ATP)} \\ + [((A_d/A_{total})(R_{a-g}) - 1)](V_g - V_a) + [((A_d/A_{total})(R_{a-s}) - 1)](V_s - V_a) \\ + I_{inj}/(A_d/A_{total})$$

where  $C_m$  is the membrane capacitance,  $A_d/A_{total}$  is the ratio of the surface area of the apical dendrite  $a$  to the total surface area of the model,  $V_a$ ,  $V_g$ , and  $V_s$  are the membrane potentials of the apical dendrite, glomerular tuft, and soma, respectively, and  $R_{a-g}$  and  $R_{a-s}$  are the linking resistances between the apical dendrite and its two neighboring compartments, the glomerular tuft and the soma, respectively. The glomerular tuft and the lateral dendrite each have only one neighboring compartment. In the simulations presented here, experimentally injected currents were inserted into the apical dendrite (to replicate experimental data based on current injection), while simulated postsynaptic currents were delivered to the distal end of the glomerular tuft (to simulate synaptic inputs). Membrane voltage recordings were made from the soma.

Ionic conductance densities in each compartment were fit using a semiautomated parameterization process broken down into two stages. First, we parameterized the model so as to replicate subthreshold activity, specifically the voltage-dependent frequency of subthreshold oscillations reported by Desmaisons et al. (1999). Six ionic conductances exhibiting voltage dependence within this narrow subthreshold voltage window ( $I_{NaP}$ ,  $I_H$ ,  $I_A$ , and  $I_{K(Ca)}$  in apical dendrite;  $I_A$  and  $I_{K(Ca)}$  in soma) were varied over a parameter space encompassing circa 60,000 combinations; the remaining conductances were held constant at existing levels. For each parameter set, the simulation was run for 13,000 ms. Starting at 3,000 ms to permit the settling of initial conditions, increasing quantities of depolarizing current were injected into the apical dendrite in steps of 1,000-ms duration, the injected current increasing in amplitude by 0.2 nA at each step. Membrane potential time series for each trial were recorded as a series

of discrete data vectors. The vectors were then analyzed using Matlab version 6.1 (The Mathworks, Natick, MA; <http://www.mathworks.com>). Each of the ~60,000 trials was broken into 11 separate time segments, each 1,000 ms in duration, corresponding to the levels of current injection and disregarding the first 2,000 ms of each simulation. The oscillation frequency for each 1,000-ms segment was taken to be the frequency at which the peak in the Fourier transform of the time series occurred. The peak frequency, mean voltage, and oscillation amplitude within each segment were measured, and all 33 calculated values (11 frequencies, 11 mean voltages, 11 mean amplitudes) for a given trial were stored as a row in the data output matrix. Using data from Desmaisons et al. (1999), a search of the output matrix of this analysis program was then performed to find a best-fit row of values, corresponding to a distinct point in the model parameter space. Second, after establishing a best-fit set of parameters for subthreshold behavior, a similar parameterization technique was used to tune the remaining active currents on the basis of the cell's observed suprathreshold activity; specifically, the number of spikes elicited per burst as a function of stimulus current. The result of this two-step procedure is the parameter set reported in Table 2.

Synaptic inputs were delivered to the distal end of the dendritic tuft compartment using NEURON's AlphaSynapse mechanism. This mechanism generates simple synaptic inputs with single-exponential kinetics and identical onset and offset time constants. GABA<sub>A</sub>-ergic inhibitory synapses were modeled with a time constant of 2.5 ms and a reversal potential of -65 mV. Glutamatergic excitatory synapses [combining AMPA and *N*-methyl-D-aspartate (NMDA) effects as discussed in RESULTS AND DISCUSSION] were modeled with a 50-ms time constant and a reversal potential of 0 mV.

## RESULTS AND DISCUSSION

We first discuss our development of the model to conform to diverse constraining datasets gathered by a number of investigators. We describe a robust region of parameter space in which the model produces complex dynamical responses replicating those observed in physiological studies. The wide range of different circumstances under which the model produces output comparable to that produced by mitral cells suggests that the model has successfully captured important features of mitral cell physiology and dynamics. We subsequently use the model to explore some mechanistic questions difficult to address in physiological preparations. In particular, we propose an explanation for the multiple forms of mitral cell bistability observed in different olfactory bulb slice preparations.

### Basic properties

Mitral cells at rest in a slice preparation exhibit mean resting potentials of -55 to -65 mV under typical recording conditions with resting potential measurements in individual cells ranging from roughly -50 to -75 mV or greater (Balu et al. 2004; Chen and Shepherd 1997; Desmaisons et al. 1999; Heyward et al. 2001; Nickell et al. 1996). Although sharp electrode recordings (Chen and Shepherd 1997; Desmaisons et al. 1999) have tended to report slightly more hyperpolarized

mean potentials ( $-62$  to  $-66$  mV) than have whole cell recordings using patch electrodes, this is approximately negated by uncompensated  $\sim 10$ -mV liquid junction potentials in the whole cell slice recordings. In *in vivo* recordings using whole cell patch electrodes, however, the mean resting potential after compensation ( $-56 \pm 1.2$  mV) was slightly more depolarized than those observed in slice preparations (Cang and Isaacson 2003). Somatic input resistance measurements have ranged between 115 and 280 M $\Omega$  in studies using patch electrodes (Cang and Isaacson 2003; Heinbockel et al. 2004; Nickell et al. 1996). At rest, the present model mitral cell exhibits a mean membrane potential of  $-64$  mV in the soma, 15-Hz subthreshold oscillations, and a somatic input resistance of 12.5 M $\Omega$ . The relatively low input resistance of the model cell is a consequence of the process of reducing its morphological complexity, during which the accurate replication of input/output properties was emphasized over the preservation of absolute parameter values (Davison et al. 2000).

Mitral cells exhibit intrinsic subthreshold membrane potential oscillations and intrinsic bursting properties, even in an olfactory bulb slice preparation and when pharmacologically

isolated with blockers of glutamatergic and GABAergic transmission (Balu et al. 2004; Chen and Shepherd 1997; Desmaisons et al. 1999). The frequency of subthreshold oscillations is highly correlated to the membrane potential, increasing in response to membrane depolarization from 10 Hz at  $-67$  mV to as high as 40 Hz at  $-59$  mV (Desmaisons et al. 1999), a phenomenon replicated by the present model (Fig. 2A). During extended stimulation, mitral cells fire clusters, or bursts, of action potentials (Fig. 2B). The number of spikes in each burst can be variable in both living and model neurons, but the spike count per burst tends to increase with increased depolarization while the interburst interval is modestly reduced (Fig. 2C) (Balu et al. 2004; Desmaisons et al. 1999). Furthermore, in the perithreshold regime, intraburst spike frequency directly reflects the frequency of subthreshold oscillations; the reduction in frequency when spikes are present is attributable to the additional potassium current activated in response to spiking (Fig. 2D). Spontaneous action potentials in mitral cells are correspondingly phase-constrained with respect to these underlying oscillations (Desmaisons et al. 1999), irrespective of their frequency (Fig. 2E).

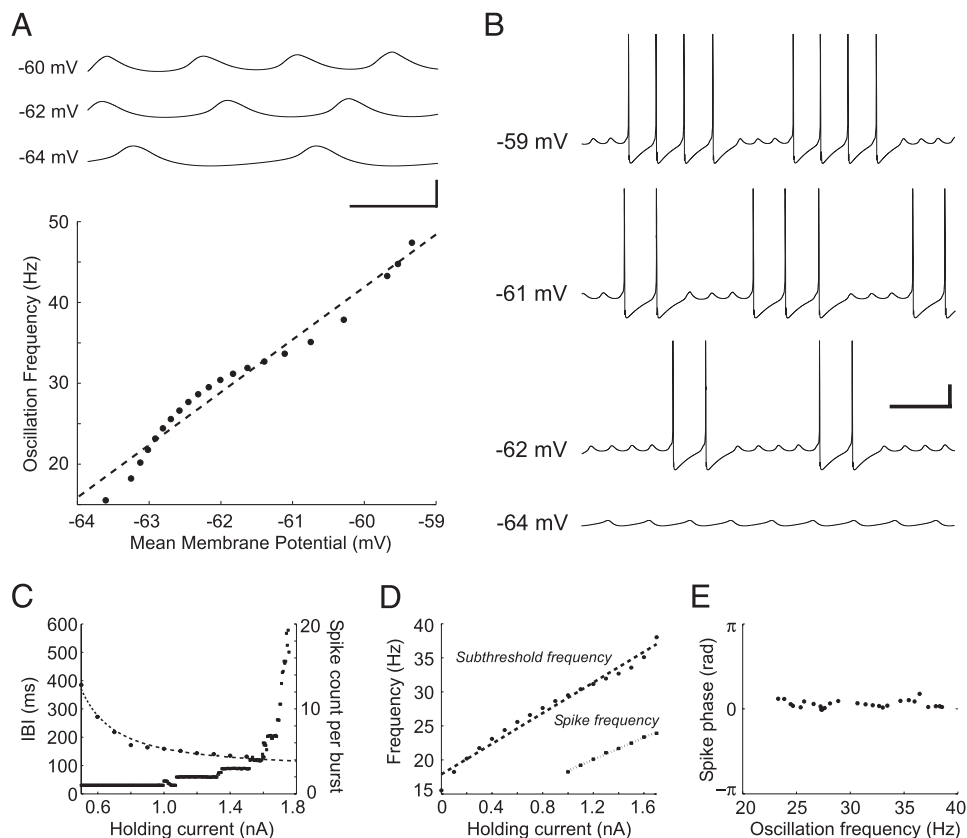


FIG. 2. Basic electrophysiological properties of the model mitral cell. *A*: frequency of subthreshold oscillations is voltage dependent. *Top*: subthreshold oscillations illustrated at 3 mean membrane potentials. *Scale bar*: 25 ms, 10 mV. Reflects Fig. 2B in Desmaisons et al. (1999). *Bottom*: oscillation frequency as a function of mean membrane potential. Reflects Fig. 2C in Desmaisons et al. (1999). *B*: depolarization via constant current injection generates bursts of action potentials. Burst durations as well as underlying oscillation frequencies are voltage dependent. Baseline membrane potentials are defined as halfway between the potentials of the peak and trough of the subthreshold oscillations. Reflects Fig. 2A in Desmaisons et al. (1999) and Fig. 1B in Balu et al. (2004). *Scale bar*: 100 ms, 25 mV. *C*: constant current injection systematically alters the interburst interval as well as the mean number of spikes per burst. Reflects Fig. 1C, *middle* and *right*, in Balu et al. (2004). *D*: constant current injection systematically affects subthreshold oscillation frequency (in the absence of sodium spike currents) and the spike frequency within bursts. Spike frequencies are slower than corresponding subthreshold oscillation frequencies owing to the recruitment of  $I_{Kf}$  and  $I_{Ks}$  delayed rectifier currents during spiking. Spike frequency is only depicted at levels of injected current evoking two or more spikes. Reflects Fig. 1C, *left*, in Balu et al. (2004). *E*: spontaneous action potentials are evoked at a consistent phase with respect to subthreshold oscillations, irrespective of their underlying frequency. The peak of the oscillation was defined as 0 radians for compatibility with the usage of Desmaisons et al. (1999).

### Phase resetting

In the perithreshold regime, spontaneous inhibitory postsynaptic currents (IPSCs) or small hyperpolarizing current pulses generate phase resets of mitral cell subthreshold oscillations, without affecting their amplitude or frequency, and can also evoke rebound spikes (Desmaisons et al. 1999). In contrast to cerebellar interneurons and Purkinje cells (Häusser and Clark 1997), the latency of evoked spikes in mitral cells is not dependent on IPSC amplitude; hence, rebound spikes evoked in mitral cells can reliably occur within restricted time windows independent of the potentially variable amplitudes of incoming IPSCs (Desmaisons et al. 1999). Notably, the latency of such a rebound spike is considerably more reliable than that of a spike evoked by a depolarizing step (Balu et al. 2004). In the present model, both small hyperpolarizing current pulses delivered to the apical dendrite and GABA<sub>A</sub>-like chloride shunt conductances opened in the glomerular tuft replicated these effects. Brief, low-amplitude hyperpolarizing pulses or inhibitory synaptic inputs reset the phase of subthreshold oscillations (Fig. 3A), whereas larger inputs could also evoke a rebound spike. Model mitral cells generated rebound spikes within narrow time windows in response to either hyperpolarizing current pulses (Fig. 3B) or synaptic shunt inhibition in the tuft (Fig. 3C) such as would be delivered by stimulus-activated periglomerular cells (Cleland and Sethupathy 2006). Characteristic of true phase resets, the latency of rebound spikes was relatively independent of the state of the mitral cell at the time of stimulation. Rebound spike timing was not strongly influenced by the baseline membrane potential or corresponding intrinsic oscillation frequency (Fig. 3D) nor by the amplitudes of the hyperpolarizing current or shunt conductance (Fig. 3E). Furthermore, spike latency was largely independent of the phase of subthreshold oscillations at the time of delivery of the current pulse (Fig. 3F) or the shunt conductance (Fig. 3G); the exception being when the inhibitory current or IPSC coincided directly with the normal phase of spike firing (0 or  $2\pi$  radians; Fig. 3, F and G).

As described in the preceding text, simulated IPSCs in the glomerular compartment, reversing at the chloride reversal potential, are capable of resetting the phase of subthreshold oscillations in the model, as they are experimentally. This observation has considerable implications for the rapid initiation of synchronized network oscillations by sensory input. Convergent OSNs directly activate both mitral cell dendrites and periglomerular cell spines; the latter then directly inhibit the former in a well-established synaptic triad (Pinching and Powell 1971; White 1972). This colocalization of excitatory and inhibitory inputs on mitral cell apical dendrites is important for the ability of periglomerular inhibition to substantially influence the response to afferent excitation (Koch et al. 1983; Liu 2004; Mel and Schiller 2004); indeed, mitral cells commonly are inhibited by odor stimuli, emphasizing the importance of such inhibitory pathways in the computation of mitral cell output (reviewed in Cleland and Sethupathy 2006). Even though mitral cell excitation by OSNs is monosynaptic whereas their inhibition via periglomerular cells is disynaptic, the depolarization of periglomerular spines and concomitant release of GABA onto mitral cell dendrites appears to precede the evocation of action potentials in mitral cells, such that chloride shunt inhibition mediated by GABA<sub>A</sub> receptors on

mitral cell apical dendrites factors into the synaptic integrative processes determining whether and when the mitral cell will fire (Cleland and Sethupathy 2006). This phenomenon is sometimes observed as a fast hyperpolarization preceding even the shortest-latency excitatory responses to odors in mitral cells (Hamilton and Kauer 1989; Kauer et al. 1990; Wellis and Scott 1990). The resulting synchronized inhibition of mitral cells across all odor-activated glomeruli will reset the phase of oscillations in all affected mitral cells, such that any spikes that may subsequently be evoked will be, to a great extent, synchronized across the active ensemble. Although appropriate connections among mitral cells are likely to be necessary to perpetuate the synchronization of their oscillations—a phenomenon largely attributed to mitral-granule interactions in the external plexiform layer—this stimulus-evoked synchronous reset generates an immediate synchronization of mitral cell intrinsic properties. In contrast, multiple cycles of excitation/inhibition coupling would likely be required for a system of coupled oscillators such as the mitral-granule network to achieve collective synchronization without such a strong phase-locking event (Strogatz 2000)—a process that would generate hundreds of milliseconds of relatively asynchronous odor-evoked mitral cell firing before the population activity became coherent.

### Subthreshold oscillations constrain spike timing

In contrast to the temporal fidelity of rebound spikes evoked by inhibitory synaptic inputs or brief hyperpolarizing pulses, action potentials evoked by excitatory synaptic inputs vary substantially in latency (Balu et al. 2004; Desmaisons et al. 1999). Specifically, while IPSCs reset the phase of subthreshold oscillation and hence evoke rebound spikes at times that are independent of the phase prior to reset, excitatory postsynaptic currents (EPSCs) do not reset phase; rather, the timings of spikes evoked by EPSCs are constrained with respect to the phase of the underlying subthreshold oscillations (Desmaisons et al. 1999). In the present model, simulated EPSCs delivered at different oscillatory phases evoked spikes with variable latencies but at a consistent phase (Fig. 4A). Specifically, EPSC-evoked spike latency depended on the phase of the excitatory stimulus (Fig. 4B), such that evoked spikes were constrained to a consistent, restricted phase window of the oscillation (Fig. 4C) in agreement with experimental data (Desmaisons et al. 1999). At modest EPSC amplitudes, these phase constraints were reliable with stronger inputs evoking spikes at shorter latencies (corresponding to a relative phase lead with respect to subthreshold oscillations). Substantially stronger EPSC amplitudes, however, were able to overpower the phasing properties of the intrinsic oscillations, evoking spikes with latencies increasingly independent of the intrinsic phase (Fig. 4D). This result suggests a particular importance for GABA<sub>B</sub>-ergic (Aroniadou-Anderjaska et al. 2000; Wachowiak et al. 2005) and D2 dopaminergic (Berkowicz and Trombley 2000; Ennis et al. 2001) presynaptic inhibition delivered onto olfactory sensory neuron terminals for the regulation of olfactory input sensitivity (McGann et al. 2005; Wei et al. 2006; Wilson and Sullivan 1995). Specifically, the resulting negative feedback loops, dynamically adjusted in gain in response to odor input activity (Philpot et al. 1998), may act to keep the intensity of afferent excitatory inputs to

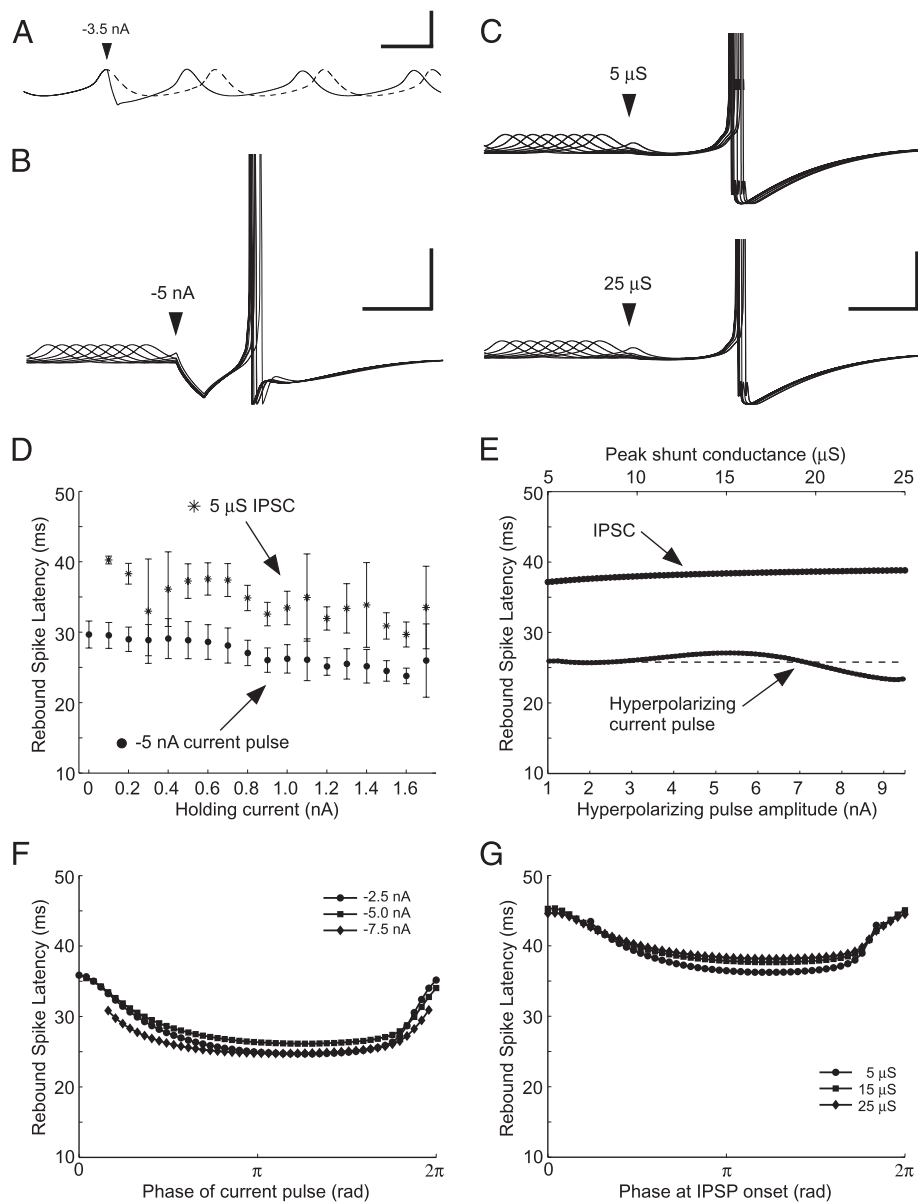


FIG. 3. Effects of inhibitory synaptic inputs. *A*: Inhibitory inputs evoke a phase reset of subthreshold oscillations. Injection of a  $-3.5$ -nA, 5-ms hyperpolarizing current pulse ( $\blacktriangledown$ ) reset the phase of subthreshold oscillations (—) compared with what their time course would have been in its absence (---). Scale bars: 25 ms, 10 mV. *B*: larger hyperpolarizing current pulses evoke rebound spikes. Eight  $-5.0$ -nA, 10-ms hyperpolarizing current pulses were injected ( $\blacktriangledown$ ) at different phases of the intrinsic oscillation, resetting the phase and evoking rebound spikes within a restricted phase window ( $\sigma \approx 1.3$  ms; range  $\approx 3.8$  ms). Baseline  $V_m = -63$  mV (owing to a constant  $+0.25$ -nA injection), corresponding to an intrinsic frequency of 21.0 Hz. Spikes are truncated. Reflects Fig. 6A in Desmaisons et al. (1999). Scale bars: 25 ms, 25 mV. *C*: chloride shunt conductances in the glomerular tuft evoke rebound spikes. Eight synaptic chloride conductances (25 pS;  $E_{Cl} = -65$  mV;  $\tau_{GABA} = 2.5$  ms) were evoked at different phases of the intrinsic oscillation ( $\blacktriangledown$ ), resetting the phase and evoking rebound spikes within a restricted phase window [ $\sigma \approx 1.2$  ms; range  $\approx 2.8$  ms; compare with 10 ms range observed by Desmaisons et al. (1999)]. Baseline  $V_m$  and intrinsic frequency as in *B*. Spikes are truncated. Reflects Fig. 6B in Desmaisons et al. (1999). Scale bars: 25 ms, 25 mV. *D*: rebound spike latencies are largely independent of baseline membrane potential (maintained with constant holding current) and the corresponding intrinsic oscillation frequency, whether evoked with hyperpolarizing current pulses ( $\bullet$ ) or chloride shunt conductances ( $*$ ), although a weak effect is visible. Variance in ordinate values is due to the unregulated phases of inhibitory postsynaptic current (IPSC) onset (uniformly distributed); error bars depict the SD based on  $50 \pm 1$  repeated simulations. Reflects Fig. 7A in Desmaisons et al. (1999). *E*: rebound spike latency is independent of the amplitudes of hyperpolarizing current pulses or inhibitory synaptic inputs (chloride conductances in the glomerular tuft). Reflects Fig. 6C in Desmaisons et al. (1999). *F*: rebound spike latency is substantially independent of the phase of onset of the hyperpolarizing current pulse. Hyperpolarizing pulses evoke spikes of relatively constant latency when delivered at most phases of the intrinsic oscillatory period, although latency is increased somewhat when the hyperpolarizing pulse is delivered during the peak of the oscillation (phase = 0 =  $2\pi$ ), when spikes are normally evoked. Note also the relative insensitivity to pulse amplitude. *G*: rebound spike latency is similarly largely independent of the phase of onset of inhibitory postsynaptic chloride conductances opened in the glomerular tuft, again excepting the peaks of subthreshold oscillations. Note also the relative insensitivity to the maximum postsynaptic conductance level.

mitral cells within this functional range so as to facilitate the intrinsic regulation of spike timing and hence the synchronization of spikes among mitral cells. Notably, within this functional range, stronger inputs are predicted to evoke leading

spikes, suggesting a downstream spike-timing based mechanism for readout of the relative intensities of glomerular activation (Cleland and Linster 2002; Linster and Cleland 2001).

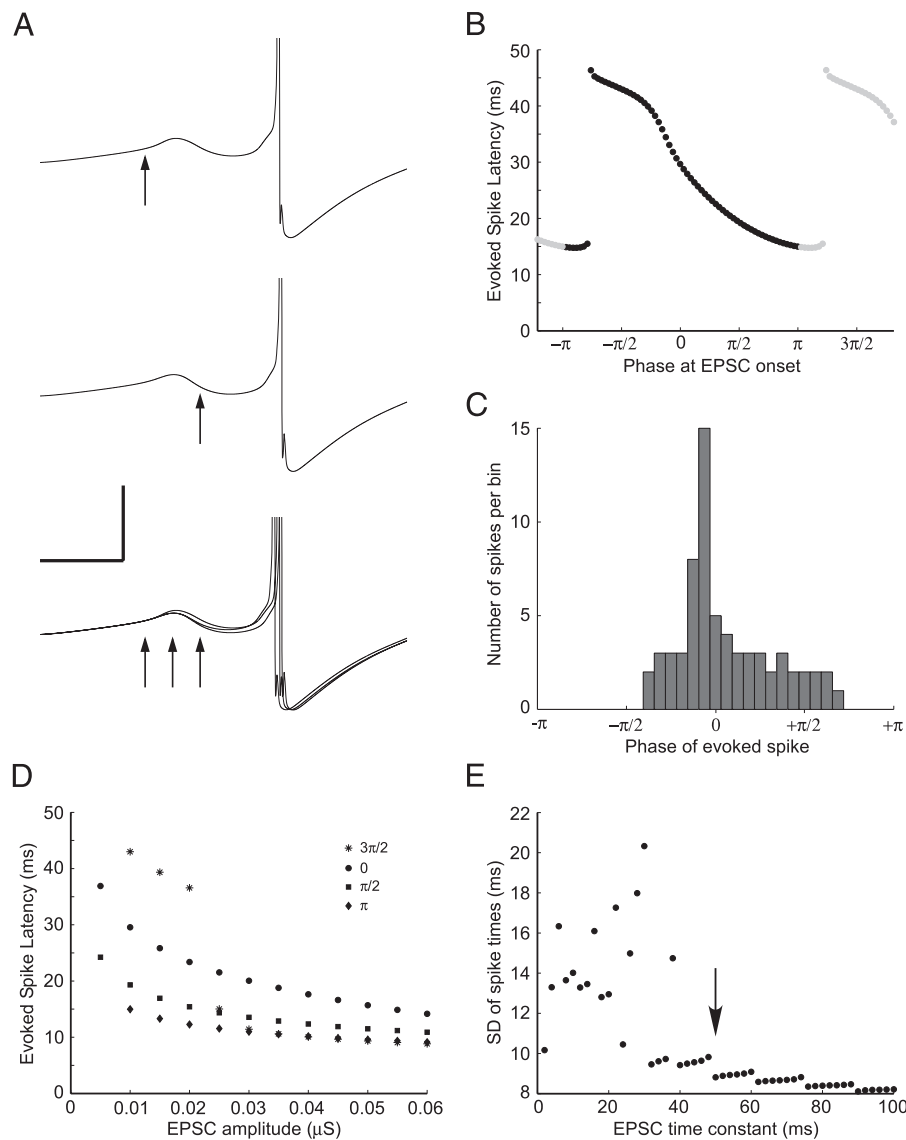


FIG. 4. Effects of excitatory synaptic inputs. Baseline membrane potential corresponds to rest ( $-64.3$  mV, intrinsic frequency of 15.2 Hz). *A, top and middle*: simulated excitatory postsynaptic currents (EPSCs) delivered at different intrinsic phases evoked spikes with variable latencies but at a consistent oscillatory phase. Reflects Fig. 8*Ba* in Desmaisons et al. (1999). *Bottom*: overlaid data from *top* and *middle* with additional input phases. Reflects Fig. 8*Bb* in Desmaisons et al. (1999). *B*: latency of EPSC-evoked spikes varies with respect to the phase of the EPSC. Data from 1 full cycle period (from  $-\pi$  to  $\pi$ ) are depicted in black; redundant data are depicted in gray to better illustrate the periodicity of this relationship. Reflects Fig. 8*Bc* in Desmaisons et al. (1999). *C*: distribution of spike times evoked by EPSCs arriving at all phases of the intrinsic oscillation period. Specifically,  $0.01 \mu\text{S}$  EPSCs were delivered at 66 uniformly distributed phases separated by 1 ms (corresponding to the 66-ms period of the oscillation). The histogram depicts the phases of the spikes evoked by these EPSCs, grouped into bins of  $\pi/16$  width. The timing of evoked spikes is strongly phase-constrained with the greatest density of spikes slightly leading the peak of the oscillation (defined as phase = 0). *D*: effect of EPSC amplitude on evoked spike latency. The effects at four phases of EPSC onset are depicted (legend). At modest amplitudes, where evoked spike latency differs depending on phase of EPSC onset, evoked spikes are phase-constrained as illustrated above. At higher EPSC amplitudes, where the curves associated with different phases of EPSC onset converge, evoked spike latency becomes increasingly independent of EPSC onset phase, indicating a reduction in the ability of intrinsic cellular oscillations to regulate spike timing. *E*: effect of EPSC time constant on the reliability of evoked spike timing. EPSC onset phase is unregulated and hence provides a source of intertrial variance. Standard deviations (ordinate) derive from spike time distributions such as that illustrated in *C*. Each point represents the SD of 34 simulation results. Fast EPSCs are relatively poor at facilitating the regulation of spike timing by intrinsic cellular oscillations. EPSCs with longer activation time constants and correspondingly shallower voltage gradients enable considerably narrower distributions of spike times, corresponding to a stricter phase constraint with respect to mitral cell intrinsic subthreshold oscillations. With the  $0.01 \mu\text{S}$  EPSC illustrated, synaptic activation time constants of roughly  $\geq 40$  ms effectively delegate authority over mitral cell spike timing to the mitral cell's intrinsic oscillations. The arrow designates the estimated time constant for afferent EPSCs in mitral cells in vivo (Ennis et al. 1998; see text).

This capacity of subthreshold oscillations to regulate the timing of evoked mitral cell spikes also depends substantially on the excitatory synaptic time constant. When excitatory synaptic currents were delivered as square pulses, evoked spike times were considerably less variable in latency and hence less constrained by oscillatory phase. Indeed the degree to which

spike timing was determined by the phase of subthreshold oscillations increased as the time constant of sensory synaptic input was lengthened; in the model, robust phase-specificity of evoked action potentials occurred when  $\tau > 30$  ms or so (Fig. 4*E*). One straightforward synthesis of these results is that synaptic potentials must be effectively slower than the intrinsic

oscillation period in order for the latter to determine spike timing (Desmaisons et al. 1999). Steeper voltage gradients ( $dV/dt$ ) are more effective at evoking action potentials than are shallower gradients; while the steep voltage gradients generated by artificial square-pulse inputs minimize the contribution of intrinsic membrane properties, the slower voltage gradients of synaptic inputs will interact with these intrinsic properties in a manner determined by their relative timescales. Interestingly, the effective time constants of afferent synaptic activation in mitral cells appear to be comfortably on a timescale that effectively delegates control over spike timing to the intrinsic subthreshold oscillations of the mitral cell (Fig. 4E, ↓). The observed peak latency for NMDA receptor-mediated synaptic potentials in mitral cells is  $82 \pm 38$  ms in response to olfactory nerve shock (Ennis et al. 1998), corresponding to a time constant of roughly 50–60 ms; additionally, metabotropic glutamatergic excitation (Ennis et al. 2006; Heinbockel et al. 2004) is likely to contribute an even slower component to the response. Rapid chloride shunt inhibition delivered by periglomerular cells may also delay odor-evoked postsynaptic depolarizations (Cleland and Sethupathy 2006), as may A-type (inactivating) potassium currents; data from granule cells show that  $I_A$  selectively attenuates the impact of fast non-NMDA glutamate receptors, such that postsynaptic depolarization follows the slower time course of the NMDA receptor (Schoppa and Westbrook 1999). The prominence of both inactivating potassium currents and fast, stimulus-evoked shunt conductances in mitral cells suggest that these effects contribute to the slow postsynaptic integration observed in these neurons.

The concordance of these phenomena enables activated mitral cells across the olfactory bulb to be rapidly synchronized by afferent inputs before evoking any action potentials. Rapid, stimulus-evoked, periglomerular cell-mediated shunt inhibition serves to reset the subthreshold oscillatory phases of mitral cells sampling from odor-activated glomeruli. The slow, concomitant excitation of these same mitral cells, if sufficient to overcome this shunt inhibition (Cleland and Sethupathy 2006), will evoke its first action potentials within a restricted phase window of these now-synchronized subthreshold oscillations, yielding an ensemble of synchronized spikes across the bulbar population of mitral cells. Notably, it is only after spikes have been evoked in activated mitral cells that mitral-granule reciprocal synapses can participate in the generation and maintenance of field oscillations.

#### *Ionic basis and pharmacology of subthreshold oscillations*

Intrinsic membrane oscillations generally comprise at least two opposing currents with interacting dependencies. Subthreshold oscillations are of course restricted to depending on currents that are differentially activated across this limited range of membrane potentials and hence often incorporate the persistent sodium current  $I_{NaP}$  as a source of excitatory drive (Agrawal et al. 2001; Dickson et al. 2000; Fransén et al. 2004; Klink and Alonso 1993; Magistretti and Alonso 1999; Manis et al. 2003; Reboreda et al. 2003; Sanhueza and Bacigalupo 2005; Wang 1993; Wu et al. 2005). Like the sodium spike current, the persistent sodium current is tetrodotoxin (TTX) sensitive. However, it does not exhibit rapid inactivation; inactivation processes in  $I_{NaP}$  are substantially slower and/or less complete (Crill 1996; Magistretti and Alonso 1999; Wu et al. 2005).

Furthermore, the activation curves for persistent sodium currents are typically displaced 7–10 mV negative to those describing the inactivating sodium spike current, hence yielding a substantial voltage window for subthreshold and perithreshold resonant activity. Finally, persistent sodium currents are small, typically contributing only 0.25% of the maximum transient sodium current (Crill 1996); this presumably helps avoid runaway depolarization by keeping the noninactivating component of the inward current comfortably under control by the cell's complement of outward currents.

Application of TTX abolishes subthreshold oscillations in mitral cells, indicating that these oscillations depend on the persistent sodium current (Balu et al. 2004; Desmaisons et al. 1999). In the model mitral cell, blocking  $G_{NaP}$  entirely abolished oscillations (Fig. 5A). In contrast, eliminating voltage-activated calcium currents from the model had no effect on subthreshold oscillations (Fig. 5A) in agreement with experimental data (Desmaisons et al. 1999).

In mitral cell subthreshold oscillations, the outward currents responsible for repolarization are likely to be potassium currents. In slice experiments, a 33% reduction in external potassium concentration resulted in larger afterhyperpolarizations (AHPs) but did not generate substantial change in the amplitude or frequency of subthreshold oscillations (Desmaisons et al. 1999). Although these authors concluded that this ruled out a role for potassium currents in the maintenance of oscillations, our model demonstrates that this response profile is consistent with the participation of potassium currents in subthreshold oscillations. The reduction of external potassium from 3 to 2 mM displaces the potassium reversal potential  $E_K$  from  $-90$  to  $-100$  mV, a change that might be expected to markedly enhance AHPs, which correspond with very high total membrane potassium conductances, without visibly influencing the small currents underlying subthreshold oscillations. Indeed, altering the potassium reversal potential in the model to correspond with this experiment substantially increased AHP amplitude (Fig. 5B) but did not markedly alter subthreshold oscillations (Fig. 5B, inset). Subsequent analyses of membrane currents in the model revealed that potassium currents were fluctuating along with subthreshold membrane potential oscillations (Fig. 5C) and were necessary for their perpetuation. Specifically, the inactivating potassium current  $I_A$  and the calcium-dependent potassium current were active at subthreshold voltages and contributed to oscillations; the delayed rectifier channels  $I_{Kf}$  and  $I_{Ks}$  were not activated at subthreshold potentials.

Direct pharmacological testing of potassium current effects under current clamp conditions is difficult, as their blockade usually results in seizure and/or excitotoxicity. We tested their contribution to the maintenance of oscillations in the model by clamping their conductances to appropriate static levels; that is, net potassium conductance levels were set so as to confer appropriate subthreshold membrane potentials but were not permitted to fluctuate, effectively converting them to ohmic leak currents reversing at  $E_K$ . Specifically, Fig. 6 depicts mitral cell activity when normally voltage-dependent currents are selectively clamped to static conductances that yield the same mean membrane potential as when the cell is at normal rest ( $-64.3$  mV, corresponding to subthreshold oscillations of 15 Hz). The clamping of either subthreshold potassium current ( $I_A$  or  $I_{K(Ca)}$ ) abolished subthreshold oscillations and bursting

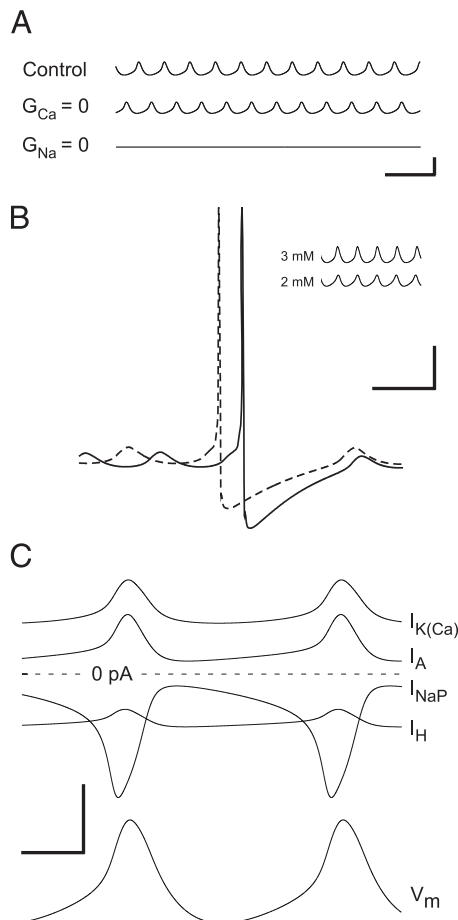


FIG. 5. Ionic basis and pharmacology of subthreshold oscillations. *A*: blockade of calcium currents ( $G_{Ca} = 0$ ; comparable to cobalt application) does not affect the amplitude or frequency of subthreshold oscillations, whereas blockade of sodium currents [ $G_{Na} = 0$ ; comparable to tetrodotoxin (TTX) application] blocks them. Reflects Fig. 4, *A* and *B*, in Desmaisons et al. (1999). Scale bars: 100 ms, 10 mV. *B*: reducing the external potassium concentration from 3 to 2 mM alters the potassium reversal potential from  $-90$  to  $-100$  mV but does not visibly affect subthreshold oscillations (*inset*); however, it markedly increases the amplitude of spike afterhyperpolarizations. - - -, 3 mM; —, 2 mM external potassium. Mean resting potential was maintained at  $-62$  mV via current injection. *Inset* and methods reflect Fig. 4*C* in Desmaisons et al. (1999). Scale bars: 25 ms, 20 mV (150 ms, 20 mV for *inset*). The time offset is arbitrary. *C*: membrane current fluctuations underlying membrane potential oscillations. Current offsets are accurate with respect to the 0-current line. Note that although all 4 currents illustrated participate in subthreshold oscillations, only 3 of them ( $I_{NaP}$ ,  $I_A$ , and  $I_{K(Ca)}$ ) are necessary for the generation of these oscillations (see Fig. 6). Scale bars: 15 ms, 10 pA, 5 mV.

properties, instead yielding tonic spiking (Fig. 6, *A–C*), the frequency of which varied monotonically with the level of clamped (ohmic) potassium current. Clamping of the persistent sodium current  $I_{NaP}$  at any level abolished all subthreshold oscillatory activity in the model cell (Fig. 6*D*). In contrast, clamping the hyperpolarization-activated inward current  $I_H$  did not impair subthreshold oscillations (Fig. 6*E*), indicating that this current is not a necessary dynamical contributor to these oscillations.

It is clear that subthreshold oscillations in the model depend on  $I_{NaP}$ ,  $I_A$ , and  $I_{K(Ca)}$  in the sense that the removal or clamping of any of these currents disrupts these oscillations. However, the degree of certainty about the role and importance of each current differs. Certainly, the persistent sodium current is

essential to the model's oscillogenic properties and has been clearly documented in pharmacological studies. The respective roles of the different outward potassium currents, however, remain unclear. Subthreshold oscillations are a low-current phenomenon; both model potassium conductances are minimally open during the course of these oscillations ( $I_A$ : no more than 1.9% of  $G_{max}$ ;  $I_{K(Ca)}$ : no more than 0.3% of  $G_{max}$ ).

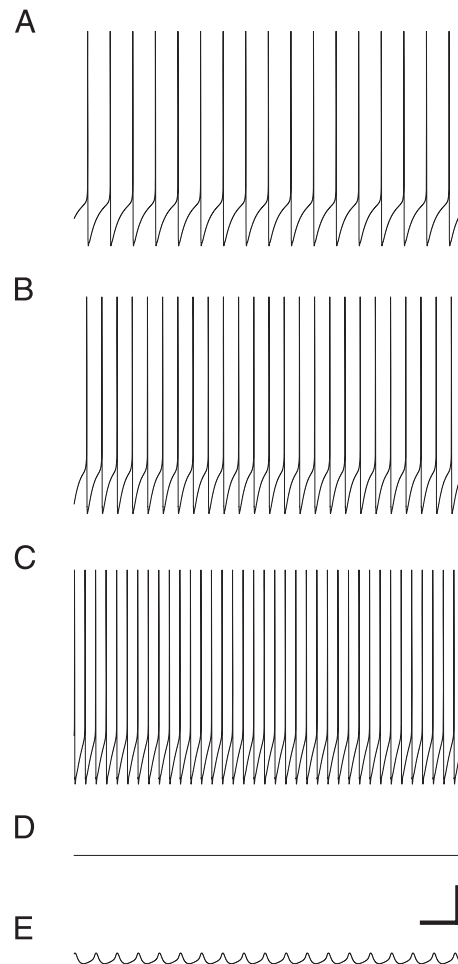


FIG. 6. Effects of clamping membrane currents involved in subthreshold oscillations. In an effort to test which membrane currents were genuinely necessary to sustain subthreshold oscillations, the 4 currents differentially active at subthreshold potentials were each clamped at a constant conductance in all compartments, rendering them ohmic. Clamping was performed in lieu of blocking (clamping to 0) so that blocking currents could not disrupt oscillations in a trivial sense by moving the cell out of the membrane potential range supporting subthreshold oscillations. Clamping conductances were chosen to achieve a mean resting potential of  $-64.3$  mV (the normal mean resting potential of the model cell). Cited conductances refer to the primary dendrite compartment; conductance ratios were maintained among compartments (Table 2). Scale bars: 100 ms, 25 mV. *A*: clamping of  $I_A$  to  $134 \mu S/cm^2$  produced tonic firing. Reducing  $I_A$  below the level shown increased firing frequency; increasing  $I_A$  reduced firing frequency until the cell became silent. *B*: clamping of  $I_{K(Ca)}$  to  $166 \mu S/cm^2$  also produced tonic firing. Reducing  $I_{K(Ca)}$  below the level shown increased spike frequency; increasing  $I_{K(Ca)}$  reduced firing frequency until the cell became silent. *C*: clamping of both  $I_A$  and  $I_{K(Ca)}$  to a net level of  $210 \mu S/cm^2$  of ohmic potassium current produced essentially the same macroscopic properties as were expressed when either current alone was clamped. *D*: clamping  $I_{NaP}$  to any level abolished subthreshold oscillations; clamping to  $45 \mu S/cm^2$  as illustrated maintained the cell at a  $-64.3$  mV resting potential. *E*: clamping of  $I_H$  to  $137 \mu S/cm^2$  did not abolish subthreshold oscillations but slightly increased their frequency to 18.3 Hz (from 15.2 Hz) and their amplitude to 6.8 mV (from 5.8 mV).

Furthermore, during subthreshold oscillations, neither the inactivation properties of  $I_A$  nor the calcium sensitivity of  $I_{K(Ca)}$  contribute significantly to the determination of total outward current. Indeed, they might be interchangeable in this role but for their different activation time constants. Of course, the two currents are well differentiated in their roles during mitral cell spiking and burst generation. Interestingly, such similarities in the properties of low-threshold potassium currents in the perithreshold regime could render mitral cell subthreshold oscillations reasonably robust to variations in the relative levels of expression of different potassium current species that might be employed to regulate suprathreshold properties such as bursting.

### Slow processes regulating burst properties

When mitral cells are continuously depolarized, they evoke repetitive bursts of action potentials, the duration and spike frequency of which depend on the degree of depolarization, as replicated by the model (Fig. 2). These intermittent bursts are dependent on 4-aminopyridine (4-AP)-sensitive currents, as application of increasing concentrations of this inactivating potassium current blocker reduces and then eliminates interburst intervals in mitral cells, eventually producing tonic activity (Balu et al. 2004). The slow process primarily responsible for the initiation and termination of bursts has not been identified but has been suggested to involve the build-up of an outward current during the burst (Balu et al. 2004).

In the present model, the slow currents regulating burst parameters include an inactivating potassium current ( $I_A$ ) with moderate inactivation kinetics, corresponding to the 4-AP-sensitive A- and/or D-type channels (Coetzee et al. 1999; Wu and Barish 1992) as well as a calcium-dependent potassium current ( $I_{K(Ca)}$ ). Both of these types of currents are prominent in mitral cells (Balu et al. 2004; Chen and Shepherd 1997; Wang et al. 1996). Blockade of A-like currents with 4-AP dramatically reduced the latency to first spike in response to step depolarization in both the slice (Balu et al. 2004) and the present model (not shown). Furthermore, when the model cell was depolarized so as to fire bursts of spikes (Fig. 7A), reduction of  $I_A$  eliminated the slow modulation underlying bursting: weak antagonism increased burst duration (not shown), whereas higher levels of blockade rendered spiking entirely tonic (Fig. 7B), as demonstrated experimentally (Balu et al. 2004). Although the model cell clearly replicates many of the salient features of burst firing in mitral cells, measurements of membrane current fluctuations in the model during bursting do not support the view that a simple build-up of potassium currents is responsible for burst termination. Indeed, most potassium current levels decline over the course of each burst with  $I_A$  being the prominent exception (Fig. 7C). Rather, simulations suggest that a progressive deinactivation of  $I_A$  over the course of a burst is the main factor terminating clusters of spikes in the model (Fig. 7D). Specifically, the recruitment of high-threshold potassium currents  $I_{Kf}$  and  $I_{Ks}$  during spiking transiently hyperpolarizes the cell between spikes to a level that favor the cumulative deinactivation of  $I_A$  until the point at which the resulting potentiation of this fast, low-threshold potassium current successfully prevents spike initiation. Of course, this theoretical hypothesis requires experimental study. For example, if calcium buffering in the model was slowed and

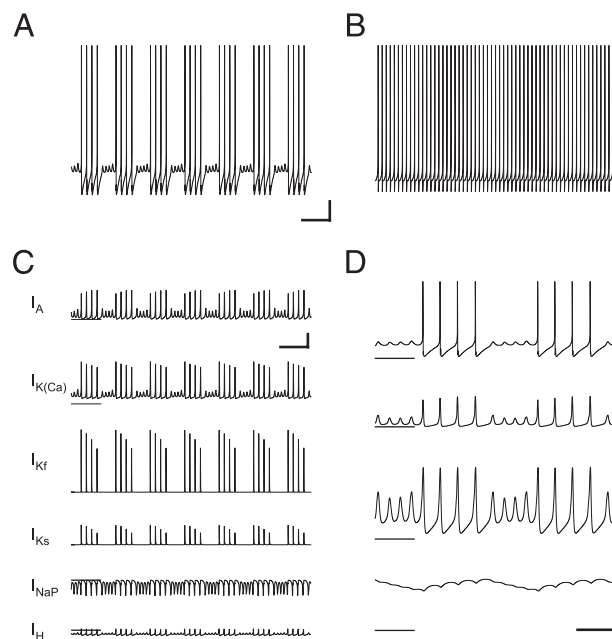


FIG. 7. Mechanisms and currents underlying mitral cell bursting. *A*: normal bursting in a mitral cell activated with 1.58 nA of steady depolarizing current. Scale bars: 250 ms, 20 mV. *B*: changes in mitral cell activity with a 50% blockade of the inactivating potassium current  $I_A$ . Slight blockade (5%) of this current increases the duration of spike bursts (not shown), whereas substantial blockade eliminates bursting entirely, reflecting Fig. 8A in Balu et al. (2004). Same scale as in *A*. *C*: time series of 6 membrane currents underlying periodic bursting, aligned with the voltage time course depicted in *A*. —, 0-current levels; the delayed rectifiers  $I_{Kf}$  and  $I_{Ks}$  flux 0 current except during spikes. Scale bars: 250 ms, 2 pA. *D*: higher temporal resolution depiction of bursting parameters: membrane voltage, A-type inactivating potassium current, and the A-current activation ( $m$ ) and inactivation ( $h$ ) parameters, each of which vary between 0 and 1. Higher levels of  $h$  connote less inactivation. These results suggest that the progressive deinactivation of  $I_A$  is a likely determinant of burst termination; notably, all other outward currents decline in amplitude over the course of a given burst. Scale bars: 100 ms, 30 mV, 20 pA, 0.2 ( $m$ ), 0.02 ( $h$ );  $m$  and  $h$  are unitless. Horizontal lines mark the 0 level for all ordinate variables.

the  $I_{K(Ca)}$  current mechanism in the present model was rendered proportionately more dependent on perimembrane calcium levels, then another modeling solution might be found in which a gradual accumulation of this current over the course of a burst is eventually responsible for its termination.

There has been considerable interest in the properties and composition of the inactivating potassium current in mitral cells. In our model, as in its predecessors, the inactivation time constant of the model A-type current is 150 ms (Bhalla and Bower 1993), a value intermediate between the ranges associated with classical fast-inactivating A current and those associated with its slower, putative variant known as D current (Wu and Barish 1992), but certainly reflecting the slower C-type inactivation mechanism nominally characteristic of the latter (Fadool and Levitan 1998; see also Kiss and Korn 1998). Direct measurements of the inactivation time constant for total endogenous A/D-like currents in mitral cells vary [45 ms (Wang et al. 1996); 90 ms (Hayar et al. 2001); 40–500 ms (Balu et al. 2004)], and it has been proposed that both A- and D-like currents—or, equivalently, a heterogeneous population of inactivating potassium currents—are maintained in mitral cells (Balu et al. 2004; Chen and Shepherd 1997). Interestingly, all such currents appear to require the Kv1.3 alpha subunit in mitral cells, as cultured mitral cells extracted from

Kv1.3 null mutant mice express essentially no inactivating potassium current (Fadool et al. 2004). As homomeric Kv1.3 channels exhibit very slow inactivation time constants (800 ms) (Fadool and Levitan 1998), the inactivating potassium channel population in mitral cells is probably largely heteromeric (see also Kues and Wunder 1992; Veh et al. 1995). Conceivably, the net inactivation time constant of a heterogeneous population of inactivating potassium currents may even be regulated by differentially expressing these stoichiometric variants.

*Infrathreshold bistability: a protective mechanism?*

In addition to subthreshold oscillations, some mitral cells exhibit another form of intrinsic bistability in their membrane potentials, spontaneously alternating between an *up* state, which is perithreshold for spike initiation and exhibits subthreshold oscillations as described in the preceding text, and an infrathreshold *down* state that is  $\sim 10$  mV more hyperpolarized and exhibits neither oscillations nor spikes (Heyward et al. 2001). However, the observation of this bistability is not uniform. Bistability is observed more often in cells positioned deeply within a slice than in more superficial cells (Heyward et al. 2001) and is consistently observed by some laboratories (Hayar et al. 2001; Heinbockel et al. 2004; Heyward et al. 2001) but rarely or never by others (Balu et al. 2004; Chen and Shepherd 1997; Desmaisons et al. 1999; Nickell et al. 1996; Urban and Sakmann 2002). In all of these studies, monostable mitral cells (i.e., those not exhibiting this infrathreshold form of bistability) exhibited properties characteristic of the up state in bistable cells, indicating that it is the presence of the down state that is inconsistently observed.

The role of infrathreshold bistability in mitral cell function, and its mechanistic relationships with other complex membrane phenomena such as subthreshold oscillations and burst properties, are not clear. We employed the present model to examine potential determinants of this infrathreshold bistability. First, it has been argued that healthy cells are more likely to display bistability, thus explaining why cells deeper within a slice, which may be less disturbed by slice preparation than more superficial neurons, are more likely to be bistable. Differences in the general health of slices across laboratories are difficult to assess; however, this hypothesis may be contraindicated in that mitral cells recorded *in vivo* have not displayed this bistability (Cang and Isaacson 2003). Second, cellular properties may differ among studies based on the age of the animals from which the slices are taken, particularly as the olfactory bulb continues to develop postnatally in rats for  $\geq 4$  wk (Altman 1969; Mair et al. 1982; Rosselli-Austin and Altman 1979; Valverde et al. 1992). However, this variable did not correlate with bistability; both bi- and monostability were observed in mitral cells taken from rats both younger (Balu et al. 2004; Hayar et al. 2001) and older (Chen and Shepherd 1997; Desmaisons et al. 1999; Heinbockel et al. 2004; Heyward et al. 2001; Nickell et al. 1996) than 28 days postnatal. Third, the presence of the down state could depend on replicable experimental factors. One such factor that correlates with the observation of mitral cell bistability is the composition of the intracellular (electrode) medium. Specifically, preparations that do not include phosphocreatine in the intracellular medium show bistability in a substantial proportion of recorded mitral

cells (Hayar et al. 2001; Heinbockel et al. 2004; Heyward et al. 2001), whereas studies that either include intracellular phosphocreatine (Balu et al. 2004; Cang and Isaacson 2003; Urban and Sakmann 2002) or utilize sharp electrodes that do not rapidly dialyze cells (Chen and Shepherd 1997; Desmaisons et al. 1999) do not display this bistability. In hippocampal CA1 neurons, inclusion of phosphocreatine attenuates a strong and rapid potassium conductance that is induced by even brief hypoxia (Chung et al. 1998), implicating a class of ATP-sensitive potassium channels long associated with such a neuroprotective role. In slice preparations, where oxygen is available only via diffusion from the oxygenated saline present at the surface, cells located more deeply within a slice preparation would be more susceptible to hypoxia and hence more likely to display this form of bistability. In this interpretation, the presence of phosphocreatine in the pipette would mitigate the hypoxia-induced disinhibition of the K(ATP) conductance, thereby reducing the probability of occurrence of the down state.

Membrane potential hyperpolarization via the disinhibition of K(ATP) channels is a common response to hypoxic insult in several resistant neurons. Hypoxia can evoke runaway depolarization in mammalian neurons, a process associated with rising intracellular calcium concentrations and the excitotoxic accumulation of extracellular glutamate as well as the rapid depletion of intracellular energy stores and eventual cell death (Ballanyi 2004; Yamada and Inagaki 2005). Persistent sodium currents in particular are increased by hypoxia, a response thought to be one of the early causal steps in this hypoxic cascade (Hammarström and Gage 2002). Some classes of neuron, however, are relatively tolerant of hypoxia, deploying a variety of strategies to counter its deleterious effects. In particular, the disinhibition of K(ATP) channels strongly hyperpolarizes cells, suppressing the propagation of epileptogenic activity across networks and rapidly limiting neuronal energy expenditure by reducing the requirement for ion pumping, which consumes roughly half of all energy used in the brain (Ballanyi 2004; Yamada and Inagaki 2005). Knockout mice lacking Kir6.2, the pore-forming subunit of the plasma membrane K(ATP) channel, are extremely susceptible to hypoxia-induced seizures (Yamada and Inagaki 2005).

Mitral cells are likely to be particularly vulnerable to excitotoxicity. Multiple positive feedback loops are embedded within the neural circuitry of the olfactory bulb, most notably self- and mutual excitation among mitral cells (Aroniadou-Anderjaska et al. 1999; Didier et al. 2001; Friedman and Strowbridge 2003; Isaacson 1999; Nicoll and Jahr 1982; Salin et al. 2001; Urban and Sakmann 2002) and among short-axon and external tufted neurons (Aungst et al. 2003; Cleland and Sethupathy 2006). Although useful when well regulated, such loops are inherently dangerous to network stability and invite runaway depolarization; indeed, the olfactory bulb can generate epileptic seizures (Araki et al. 1995; McEvoy et al. 2002), a vulnerability that may contribute to multiple chemical-sensitivity disorders (Gilbert 2001). Furthermore, mitral cells receive direct excitatory inputs from OSNs, which are both highly convergent on mitral cell dendrites and extremely vulnerable to environmental insult, potentially leading to the rapid and uncontrolled release of glutamate onto mitral cell dendrites as compromised OSNs depolarize and die. Indeed, immunohistochemical and *in situ* hybridization studies reveal intense

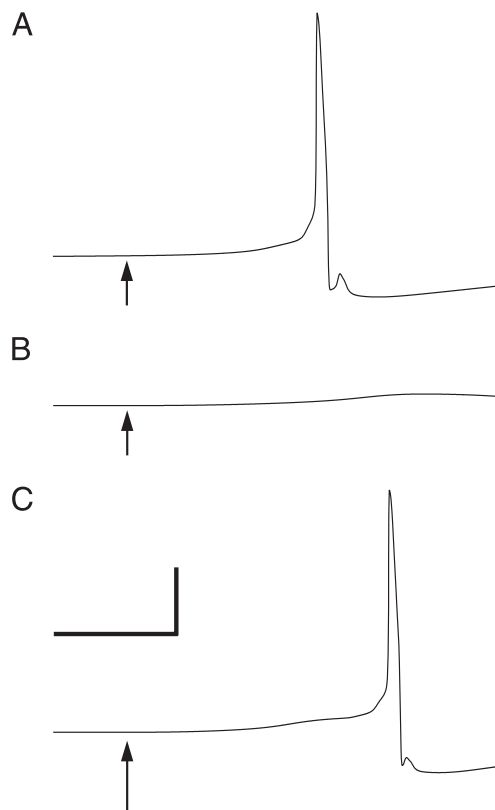


FIG. 8. Activation of an ohmic potassium current  $I_{K(ATP)}$  generates a down-state. *A*: modest ( $0.01 \mu S$ ) excitatory synaptic input evokes an action potential. *B*: after activation of a  $0.1 \text{ mS/cm}^2$  ATP-dependent potassium current, representing a transition to the down-state in response to hypoxic conditions, the same excitatory input fails to evoke an action potential. *C*: under the same conditions as in *B*, a substantially larger excitatory input ( $0.04 \mu S$ ) is able to evoke an action potential from the down-state, albeit with a longer latency. Reflects Fig. 6 in Heyward et al. (2001). Scale bars: 5 ms, 20 mV.

staining for Kir6.2 in olfactory bulb mitral and tufted cells (Zhou et al. 2002), confirming the expression of K(ATP) channels therein and suggesting that this anti-excitotoxic mechanism is present and functional in mitral cells.

Using the model, we tested whether the activation of an ohmic potassium conductance ( $I_{K(ATP)}$ ) could suffice to generate a down state. Indeed, on activation of a modest K(ATP) conductance (Table 2), the resting potential of the model mitral cell became more hyperpolarized and subthreshold oscillations ceased. Excitatory synaptic inputs normally sufficient to evoke spiking activity (Fig. 8*A*) failed to do so after  $I_{K(ATP)}$  activation (Fig. 8*B*), although this inhibition could be overcome by stronger excitatory inputs (Fig. 8*C*) as has been demonstrated experimentally (Heyward et al. 2001). These effects confirm the sufficiency of an  $I_{K(ATP)}$ -like disinhibition mechanism to suppress potentially excitotoxic synaptic inputs in mitral cells. Other observed physiological properties of bistable mitral cells, such as the slow progression from the down to the up state and the voltage-dependent properties that govern the transitions between the two states (Heyward et al. 2001), could be mediated by a number of factors, such as the declining disinhibition of K(ATP) current while in the down state because of lower ATP consumption coupled with the hypoxic potentiation of persistent sodium currents (Hammarström and Gage 2002). However, hypoxia can exert multiple and complex

effects on the properties of membrane channels (Lopez-Barneo et al. 2001), so it remains unclear which mechanisms would be primarily responsible for the complex properties of this form of bistability. It does suggest, however, that certain membrane mechanisms such as K(ATP) channels may not be contributing to odor coding per se but rather may mediate other functions necessary for the maintenance and stable operation of the olfactory system.

### Synthesis

When convergent OSNs become activated, mitral cells receive direct excitatory inputs via ionotropic and metabotropic glutamate receptors as well as indirect shunt inhibition via periglomerular cells. It has long been known that even the fastest mitral cells are delayed in their responses to odor stimuli; although some of this delay is clearly due to physical factors inherent in sniffing behavior as well as odorant diffusion across the mucus layer, additional delay also can be attributed to mitral cells' relatively slow rise toward spike threshold. This slow progress toward threshold has two consequences that bear on current theories of bulbar function. First, it provides a window of time for disynaptic shunt inhibition via periglomerular cells to exert its effects on mitral cell integration before direct monosynaptic excitation can evoke action potentials (Cleland and Sethupathy 2006), an effect sometimes observed as a fast hyperpolarization immediately preceding even the shortest-latency mitral cell responses to odors (Hamilton and Kauer 1989; Kauer et al. 1990; Wellis and Scott 1990). These IPSCs will reset the phase of subthreshold oscillations in activated mitral cells, rapidly synchronizing the activated mitral cell population. Second, among mitral cells activated strongly enough to overcome this shunt inhibition, the relatively slow progress of depolarization largely delegates the determination of mitral cell spike timing to the intrinsic oscillatory phase of their subthreshold oscillations. As the mitral cell population is by this point transiently synchronized, the spikes evoked by activated mitral cells will also be correspondingly synchronized, perhaps with more strongly activated mitral cells enjoying a slight phase lead. This synchronized activation of mitral cells presumably contributes strongly to the initiation of network oscillations among mitral and granule cells that further regulate the bulbar response to odorant stimulation. In sum, the intrinsic properties of mitral cells, coupled with the circuitry of the glomerular synaptic triad, may comprise an effective engine for translating patterns of rate-coded primary olfactory receptor activity into a timing-dependent secondary representation (Cleland and Linster 2002; Linster and Cleland 2001) that is likely to be considerably more metabolically efficient (Baddeley et al. 1997; Balasubramanian et al. 2001; Levy and Baxter 1996; Schreiber et al. 2002) and appropriate for broad distribution within the brain (Cleland and Linster 2003).

### ACKNOWLEDGMENTS

We are grateful to C. Linster, M. Ennis, A. Keller, and B. Strowbridge for technical discussions and comments and to T. Carnevale for technical advice regarding NEURON.

### GRANTS

This work was supported by National Institute on Deafness and Other Communication Disorders Grants DC-005727 and DC-007725 to T. A. Cleland.

## REFERENCES

- Agrawal N, Hamam BN, Magistretti J, Alonso A, and Ragsdale DS. Persistent sodium channel activity mediates subthreshold membrane potential oscillations and low-threshold spikes in rat entorhinal cortex layer V neurons. *Neuroscience* 102: 53–64, 2001.
- Altman J. Autoradiographic and histological studies of postnatal neurogenesis. IV. Cell proliferation and migration in the anterior forebrain, with special reference to persisting neurogenesis in the olfactory bulb. *J Comp Neurol* 137: 433–457, 1969.
- Araki T, Kato M, and Kobayashi T. Limbic seizures originating in the olfactory bulb: an electro-behavioral and glucose metabolism study. *Brain Res* 693: 207–216, 1995.
- Aroniadou-Anderjaska V, Ennis M, and Shipley MT. Dendrodendritic recurrent excitation in mitral cells of the rat olfactory bulb. *J Neurophysiol* 82: 489–494, 1999.
- Aroniadou-Anderjaska V, Zhou FM, Priest CA, Ennis M, and Shipley MT. Tonic and synaptically evoked presynaptic inhibition of sensory input to the rat olfactory bulb via GABA(B) heteroreceptors. *J Neurophysiol* 84: 1194–1203, 2000.
- Aungst JL, Heyward PM, Puche AC, Karnup SV, Hayar A, Szabo G, and Shipley MT. Centre-surround inhibition among olfactory bulb glomeruli. *Nature* 426: 623–629, 2003.
- Baddeley R, Abbott LF, Booth MC, Sengpiel F, Freeman T, Wakeman EA, and Rolls ET. Responses of neurons in primary and inferior temporal visual cortices to natural scenes. *Proc Biol Sci* 264: 1775–1783, 1997.
- Balasubramanian V, Kimber D, and Berry MJ, 2nd. Metabolically efficient information processing. *Neural Comput* 13: 799–815, 2001.
- Ballanyi K. Protective role of neuronal KATP channels in brain hypoxia. *J Exp Biol* 207: 3201–3212, 2004.
- Balu R, Larimer P, and Strowbridge BW. Phasic stimuli evoke precisely timed spikes in intermittently discharging mitral cells. *J Neurophysiol* 92: 743–753, 2004.
- Berkowicz DA and Trombley PQ. Dopaminergic modulation at the olfactory nerve synapse. *Brain Res* 855: 90–99, 2000.
- Bhalla US and Bower JM. Exploring parameter space in detailed single neuron models: simulations of the mitral and granule cells of the olfactory bulb. *J Neurophysiol* 69: 1948–1965, 1993.
- Cang J and Isaacson JS. In vivo whole-cell recording of odor-evoked synaptic transmission in the rat olfactory bulb. *J Neurosci* 23: 4108–4116, 2003.
- Carnevale NT and Hines ML. *The NEURON Book*. Cambridge: Cambridge, 2006.
- Chen WR and Shepherd GM. Membrane and synaptic properties of mitral cells in slices of rat olfactory bulb. *Brain Res* 745: 189–196, 1997.
- Chung I, Zhang Y, Eubanks JH, and Zhang L. Attenuation of hypoxic current by intracellular applications of ATP regenerating agents in hippocampal CA1 neurons of rat brain slices. *Neuroscience* 86: 1101–1107, 1998.
- Cleland TA and Linster C. How synchronization properties among second-order sensory neurons can mediate stimulus salience. *Behav Neurosci* 116: 212–221, 2002.
- Cleland TA and Linster C. Central olfactory processing. In: *Handbook of Olfaction and Gustation*, edited by Doty RL. New York: Dekker, 2003, p. 165–180.
- Cleland TA and Linster C. Computation in the olfactory system. *Chem Senses* 30: 801–813, 2005.
- Cleland TA and Sethupathy P. Non-topographical contrast enhancement in the olfactory bulb. *BMC Neurosci* 7: 7, 2006.
- Coetzee WA, Amarillo Y, Chiu J, Chow A, Lau D, McCormack T, Moreno H, Nadal MS, Ozaita A, Pountney D, Saganich M, Vega-Saenz de Miera E, and Rudy B. Molecular diversity of K<sup>+</sup> channels. *Ann NY Acad Sci* 868: 233–285, 1999.
- Crill WE. Persistent sodium current in mammalian central neurons. *Annu Rev Physiol* 58: 349–362, 1996.
- Davidson AP, Feng J, and Brown D. A reduced compartmental model of the mitral cell for use in network models of the olfactory bulb. *Brain Res Bull* 51: 393–399, 2000.
- Desmaisons D, Vincent JD, and Lledo PM. Control of action potential timing by intrinsic subthreshold oscillations in olfactory bulb output neurons. *J Neurosci* 19: 10727–10737, 1999.
- Destexhe A, Contreras D, and Steriade M. Mechanisms underlying the synchronizing action of corticothalamic feedback through inhibition of thalamic relay cells. *J Neurophysiol* 79: 999–1016, 1998.
- Dickson CT, Magistretti J, Shalinsky MH, Fransén E, Hasselmo ME, and Alonso A. Properties and role of I(h) in the pacing of subthreshold oscillations in entorhinal cortex layer II neurons. *J Neurophysiol* 83: 2562–2579, 2000.
- Didier A, Carleton A, Bjaalie JG, Vincent JD, Ottersen OP, Storm-Mathisen J, and Lledo PM. A dendrodendritic reciprocal synapse provides a recurrent excitatory connection in the olfactory bulb. *Proc Natl Acad Sci USA* 98: 6441–6446, 2001.
- Ennis M, Linster C, Aroniadou-Anderjaska V, Ciombor K, and Shipley MT. Glutamate and synaptic plasticity at mammalian primary olfactory synapses. *Ann NY Acad Sci* 855: 457–466, 1998.
- Ennis M, Zhou FM, Ciombor KJ, Aroniadou-Anderjaska V, Hayar A, Borrelli E, Zimmer LA, Margolis F, and Shipley MT. Dopamine D2 receptor-mediated presynaptic inhibition of olfactory nerve terminals. *J Neurophysiol* 86: 2986–2997, 2001.
- Ennis M, Zhu M, Heinbockel T, and Hayar A. Olfactory nerve-evoked, metabotropic glutamate receptor-mediated synaptic responses in rat olfactory bulb mitral cells. *J Neurophysiol* 95: 2233–2241, 2006.
- Fadool DA and Levitan IB. Modulation of olfactory bulb neuron potassium current by tyrosine phosphorylation. *J Neurosci* 18: 6126–6137, 1998.
- Fadool DA, Tucker K, Perkins R, Fasciani G, Thompson RN, Parsons AD, Overton JM, Koni PA, Flavell RA, and Kaczmarek LK. Kv1.3 channel gene-targeted deletion produces “Super-Smeller Mice” with altered glomeruli, interacting scaffolding proteins, and biophysics. *Neuron* 41: 389–404, 2004.
- Fransén E, Alonso AA, Dickson CT, Magistretti J, and Hasselmo ME. Ionic mechanisms in the generation of subthreshold oscillations and action potential clustering in entorhinal layer II stellate neurons. *Hippocampus* 14: 368–384, 2004.
- Friedman D and Strowbridge BW. Both electrical and chemical synapses mediate fast network oscillations in the olfactory bulb. *J Neurophysiol* 89: 2601–2610, 2003.
- Gilbert ME. Does the kindling model of epilepsy contribute to our understanding of multiple chemical sensitivity? *Ann NY Acad Sci* 933: 68–91, 2001.
- Hamilton KA and Kauer JS. Patterns of intracellular potentials in salamander mitral/tufted cells in response to odor stimulation. *J Neurophysiol* 62: 609–625, 1989.
- Hammarström AK and Gage PW. Hypoxia and persistent sodium current. *Eur Biophys J* 31: 323–330, 2002.
- Häusser M and Clark BA. Tonic synaptic inhibition modulates neuronal output pattern and spatiotemporal synaptic integration. *Neuron* 19: 665–678, 1997.
- Hayar A, Heyward PM, Heinbockel T, Shipley MT, and Ennis M. Direct excitation of mitral cells via activation of alpha1-noradrenergic receptors in rat olfactory bulb slices. *J Neurophysiol* 86: 2173–2182, 2001.
- Hayar A, Shipley MT, and Ennis M. Olfactory bulb external tufted cells are synchronized by multiple intraglomerular mechanisms. *J Neurosci* 25: 8197–8208, 2005.
- Heinbockel T, Heyward P, Conquet F, and Ennis M. Regulation of main olfactory bulb mitral cell excitability by metabotropic glutamate receptor mGluR1. *J Neurophysiol* 92: 3085–3096, 2004.
- Heyward P, Ennis M, Keller A, and Shipley MT. Membrane bistability in olfactory bulb mitral cells. *J Neurosci* 21: 5311–5320, 2001.
- Hines ML and Carnevale NT. The NEURON simulation environment. *Neural Comput* 9: 1179–1209, 1997.
- Hines ML and Carnevale NT. NEURON: a tool for neuroscientists. *Neuroscientist* 7: 123–135, 2001.
- Hodgkin AL and Huxley AF. A quantitative description of membrane current and its application to conduction and excitation in nerve. *J Physiol* 117: 500–544, 1952.
- Isaacson JS. Glutamate spillover mediates excitatory transmission in the rat olfactory bulb. *Neuron* 23: 377–384, 1999.
- Kashiwadani H, Sasaki YF, Uchida N, and Mori K. Synchronized oscillatory discharges of mitral/tufted cells with different molecular receptive ranges in the rabbit olfactory bulb. *J Neurophysiol* 82: 1786–1792, 1999.
- Kauer JS, Hamilton KA, Neff SR, and Cinelli AR. Temporal patterns of membrane potential in the olfactory bulb observed with intracellular recording and voltage-sensitive dye imaging: early hyperpolarization. In: *Chemoreception: Sensory Information Processing*, edited by Schild D. Berlin: Springer-Verlag, 1990, p. 305–314.
- Kiss L and Korn SJ. Modulation of C-type inactivation by K<sup>+</sup> at the potassium channel selectivity filter. *Biophys J* 74: 1840–1849, 1998.

- Klink R and Alonso A.** Ionic mechanisms for the subthreshold oscillations and differential electroresponsiveness of medial entorhinal cortex layer II neurons. *J Neurophysiol* 70: 144–157, 1993.
- Koch C, Poggio T, and Torre V.** Nonlinear interactions in a dendritic tree: localization, timing, and role in information processing. *Proc Natl Acad Sci USA* 80: 2799–2802, 1983.
- Kues WA and Wunder F.** Heterogeneous expression patterns of mammalian potassium channel genes in developing and adult rat brain. *Eur J Neurosci* 4: 1296–1308, 1992.
- Lagier S, Carleton A, and Lledo PM.** Interplay between local GABAergic interneurons and relay neurons generates gamma oscillations in the rat olfactory bulb. *J Neurosci* 24: 4382–4392, 2004.
- Levy WB and Baxter RA.** Energy efficient neural codes. *Neural Comput* 8: 531–543, 1996.
- Linster C and Cleland TA.** How spike synchronization among olfactory neurons can contribute to sensory discrimination. *J Comput Neurosci* 10: 187–193, 2001.
- Liu G.** Local structural balance and functional interaction of excitatory and inhibitory synapses in hippocampal dendrites. *Nat Neurosci* 7: 373–379, 2004.
- Lopez-Barneo J, Pardal R, and Ortega-Saenz P.** Cellular mechanism of oxygen sensing. *Annu Rev Physiol* 63: 259–287, 2001.
- Magistretti J and Alonso A.** Biophysical properties and slow voltage-dependent inactivation of a sustained sodium current in entorhinal cortex layer-II principal neurons: a whole-cell and single-channel study. *J Gen Physiol* 114: 491–509, 1999.
- Mair RG, Gellman RL, and Gesteland RC.** Postnatal proliferation and maturation of olfactory bulb neurons in the rat. *Neuroscience* 7: 3105–3116, 1982.
- Manis PB, Molitor SC, and Wu H.** Subthreshold oscillations generated by TTX-sensitive sodium currents in dorsal cochlear nucleus pyramidal cells. *Exp Brain Res* 153: 443–451, 2003.
- McEvoy AW, Bartolucci M, Revesz T, and Harkness W.** Intractable epilepsy and olfactory bulb hamartoma. A case report. *Stereotact Funct Neurosurg* 79: 88–93, 2002.
- McGann JP, Pirez N, Gainey MA, Muratore C, Elias AS, and Wachowiak M.** Odorant representations are modulated by intra- but not interglomerular presynaptic inhibition of olfactory sensory neurons. *Neuron* 48: 1039–1053, 2005.
- Mel BW and Schiller J.** On the fight between excitation and inhibition: location is everything. *Sci STKE* 2004: PE44, 2004.
- Nickell WT, Shipley MT, and Behbehani MM.** Orthodromic synaptic activation of rat olfactory bulb mitral cells in isolated slices. *Brain Res Bull* 39: 57–62, 1996.
- Nicoll RA and Jahr CE.** Self-excitation of olfactory bulb neurones. *Nature* 296: 441–444, 1982.
- Nusser Z, Kay LM, Laurent G, Homanics GE, and Mody I.** Disruption of GABA(A) receptors on GABAergic interneurons leads to increased oscillatory power in the olfactory bulb network. *J Neurophysiol* 86: 2823–2833, 2001.
- Philpot BD, Men D, McCarty R, and Brunjes PC.** Activity-dependent regulation of dopamine content in the olfactory bulbs of naris-occluded rats. *Neuroscience* 85: 969–977, 1998.
- Pinching AJ and Powell TP.** The neuropil of the glomeruli of the olfactory bulb. *J Cell Sci* 9: 347–377, 1971.
- Reboreda A, Sanchez E, Romero M, and Lamas JA.** Intrinsic spontaneous activity and subthreshold oscillations in neurones of the rat dorsal column nuclei in culture. *J Physiol* 551: 191–205, 2003.
- Rosselli-Austin L and Altman J.** The postnatal development of the main olfactory bulb of the rat. *J Dev Physiol* 1: 295–313, 1979.
- Salin PA, Lledo PM, Vincent JD, and Charpak S.** Dendritic glutamate autoreceptors modulate signal processing in rat mitral cells. *J Neurophysiol* 85: 1275–1282, 2001.
- Sanhueza M and Bacigalupo J.** Intrinsic subthreshold oscillations of the membrane potential in pyramidal neurons of the olfactory amygdala. *Eur J Neurosci* 22: 1618–1626, 2005.
- Saraga F, Wu CP, Zhang L, and Skinner FK.** Active dendrites and spike propagation in multi-compartment models of oriens-lacunosum/moleculare hippocampal interneurons. *J Physiol* 552: 673–689, 2003.
- Schoppa NE and Westbrook GL.** Regulation of synaptic timing in the olfactory bulb by an A-type potassium current. *Nat Neurosci* 2: 1106–1113, 1999.
- Schreiber S, Machens CK, Herz AV, and Laughlin SB.** Energy-efficient coding with discrete stochastic events. *Neural Comput* 14: 1323–1346, 2002.
- Strogatz SH.** From Kuramoto to Crawford: exploring the onset of synchronization in populations of coupled oscillators. *Physica D* 143: 1–20, 2000.
- Urban NN and Sakmann B.** Reciprocal intraglomerular excitation and intra- and interglomerular lateral inhibition between mouse olfactory bulb mitral cells. *J Physiol* 542: 355–367, 2002.
- Valverde F, Santacana M, and Heredia M.** Formation of an olfactory glomerulus: morphological aspects of development and organization. *Neuroscience* 49: 255–275, 1992.
- Veh RW, Lichtinghagen R, Sewing S, Wunder F, Grumbach IM, and Pongs O.** Immunohistochemical localization of five members of the Kv1 channel subunits: contrasting subcellular locations and neuron-specific colocalizations in rat brain. *Eur J Neurosci* 7: 2189–2205, 1995.
- Wachowiak M, McGann JP, Heyward PM, Shao Z, Puche AC, and Shipley MT.** Inhibition of olfactory receptor neuron input to olfactory bulb glomeruli mediated by suppression of presynaptic calcium influx. *J Neurophysiol* 94: 2700–2712, 2005.
- Wang XJ.** Ionic basis for intrinsic 40 Hz neuronal oscillations. *Neuroreport* 5: 221–224, 1993.
- Wang XY, McKenzie JS, and Kemm RE.** Whole-cell K<sup>+</sup> currents in identified olfactory bulb output neurones of rats. *J Physiol* 490: 63–77, 1996.
- Wei CJ, Linster C, and Cleland TA.** Dopamine D2 receptor activation modulates perceived odor intensity. *Behav Neurosci* 120: 2006.
- Wellis DP and Scott JW.** Intracellular responses of identified rat olfactory bulb interneurons to electrical and odor stimulation. *J Neurophysiol* 64: 932–947, 1990.
- White EL.** Synaptic organization in the olfactory glomerulus of the mouse. *Brain Res* 37: 69–80, 1972.
- Wilson DA and Sullivan RM.** The D2 antagonist spiperone mimics the effects of olfactory deprivation on mitral/tufted cell odor response patterns. *J Neurosci* 15: 5574–5581, 1995.
- Wu N, Enomoto A, Tanaka S, Hsiao CF, Nykamp DQ, Izhikevich E, and Chandler SH.** Persistent sodium currents in mesencephalic v neurons participate in burst generation and control of membrane excitability. *J Neurophysiol* 93: 2710–2722, 2005.
- Wu RL and Barish ME.** Two pharmacologically and kinetically distinct transient potassium currents in cultured embryonic mouse hippocampal neurons. *J Neurosci* 12: 2235–2246, 1992.
- Yamada K and Inagaki N.** Neuroprotection by KATP channels. *J Mol Cell Cardiol* 38: 945–949, 2005.
- Zhou M, Tanaka O, Suzuki M, Sekiguchi M, Takata K, Kawahara K, and Abe H.** Localization of pore-forming subunit of the ATP-sensitive K(+) channel, Kir6.2, in rat brain neurons and glial cells. *Brain Res Mol Brain Res* 101: 23–32, 2002.